180 J. Phys. Chem. B **2003,** *107,* 180−185

High-Pressure ^{129}Xe NMR Study of Xenon Confined in the Nanochannels of Solid (±)-[Co(en)$_3$]Cl$_3$

Takahiro Ueda,*[†,‡] Taro Eguchi,[†] Nobuo Nakamura,[†] and Roderick E. Wasylishen*[‡]

Department of Chemistry, Graduate School of Science, Osaka University, Toyonaka, Osaka 560-0043, Japan, and Department of Chemistry, University of Alberta, Edmonton, Alberta, Canada T6G 2G2

Received: July 19, 2002; In Final Form: October 17, 2002

High-pressure ^{129}Xe NMR measurements were carried out on dehydrated (±)-[Co(en)$_3$]Cl$_3$ to investigate the pore size as well as the local structure about the confined xenon atoms. At xenon gas pressures of 0.3 MPa, the xenon chemical shift was orientation dependent, exhibiting an axially symmetric powder pattern with $\delta_{11} = 280$ ppm and $\delta_{22} = \delta_{33} = 180$ ppm. Proton to ^{129}Xe cross-polarization (CP) experiments selectively enhanced the portion of the powder pattern corresponding to $\delta_{22} = \delta_{33} = \delta_{\perp}$, confirming that the unique component of the chemical shift tensor, $\delta_{11} = \delta_{\|}$, lies along the pore axis. The isotropic chemical shift δ_{iso} at the zero pressure limit was found to be 212 ppm, and suggested a pore diameter of approximately 0.47 nm. This agrees well with the diameter of 0.44 nm estimated from the crystal structure. On increasing the pressure to 6.5 MPa, $\delta_{\perp}$ increased from 180 to 220 ppm, whereas $\delta_{\|}$ was found to be almost independent of pressure. The increase in $\delta_{\perp}$ with pressure is attributed to Xe−Xe interactions. The paramagnetic shift in the xenon chemical tensor component perpendicular to the nanochannels with increasing pressure is in accord with the recent theoretical predictions of Jameson and de Dios (*J. Chem. Phys.* **2002**, *116*, 3805) and Jameson (*J. Chem. Phys.* **2002**, *116*, 8912).

Introduction

Xenon-129 NMR spectroscopy is one of the most powerful tools available to study the pore and local structure of porous materials.[1−11] Xenon has a van der Waals diameter of 0.432 nm, comparable in size to methane molecules (van der Waals diameter of 0.450 nm). The atomic diameter of xenon enables it to enter almost any porous material. Isotropic ^{129}Xe NMR chemical shifts for atomic xenon vary over more than 300 ppm depending on the physical and chemical environment of the xenon atoms. Particularly important has been the observation that the ^{129}Xe chemical shift in confined spaces depends strongly on the size and shape of the cavity. For these reasons, ^{129}Xe NMR has been extensively applied to investigate the local environment of xenon in pores as well as to characterize the porosity of a great number of systems such as zeolites,[6−8] glasses,[9] fullerenes,[10] carbon nanotubes,[11] polymers,[12−15] and clathrate compounds,[1,16−18] as well as proteins in solution[19,20] and liquid crystals.[21, 22]

In ^{129}Xe NMR studies of porous materials, the isotropic chemical shift δ_{iso} as well as the span and skew of the chemical shift tensor are the most important parameters for characterization of the pore structure. At the zero pressure limit, δ_{iso} is known to be dominated by xenon−wall interactions, and correlates with the free volume of the pore. Fraissard et al. have studied a number of porous materials with nanochannels using ^{129}Xe NMR, and proposed a correlation between δ_{iso} and the pore diameter.[23] If an anisotropic chemical shift powder pattern is observed, the principal components of the chemical shift tensor provide information about the symmetry of the pore. In several materials with end-capped anisotropic cavities[1,24] and/or one-dimensional nanopores,[25−28] anisotropic ^{129}Xe magnetic shielding has been observed under conditions of slow exchange of xenon atoms in and out of the cavities or nanopores. In these pore systems, the symmetry of the pore space is reflected in the span and skew of the chemical shift tensor. For more than a decade, hyperpolarized (HP) xenon NMR techniques have been developed to enhance the sensitivity of ^{129}Xe NMR.[29,30] HP Xe is generated by optically pumping Rb(g) in the presence of Xe(g) with 795 nm laser irradiation. The ^{129}Xe nuclear spins are polarized through hyperfine coupling to the unpaired polarized electron spins of Rb atoms. Since this technique can enhance the polarization of Xe nuclear spins up to 5% or more, it is possible to study nanopores and surfaces with high sensitivity. Thus, hyperpolarized xenon NMR has been used to investigate the xenon−surface and xenon−wall interactions in many interesting systems.[31−42]

Almost all the previous studies employing ^{129}Xe NMR have been applied to materials which strongly absorb xenon gas at equilibrium pressures less than 0.1 MPa. In such systems, ^{129}Xe NMR measurements are relatively straightforward. The possibility of performing ^{129}Xe NMR experiments at xenon pressures well beyond 0.1 MPa would clearly expand the number of systems one could probe. Recently, Nagasaka et al. have described a conventional in situ variable pressure NMR probe, allowing studies with pressures up to 20 MPa.[15] This ^{129}Xe NMR probe has been used to characterize the free volumes of synthetic polymers with high equilibrium pressures.[15] High-pressure in situ ^{129}Xe NMR studies indicate that xenon atoms confined in the nanopores of polymers are strongly affected by the xenon−wall interactions, and that the ^{129}Xe chemical shifts of the confined xenon atoms are not influenced by the drastic change of the free xenon density in the critical region.[15] ^{129}Xe

---

* To whom correspondence should be addressed. Takahiro Ueda (Phone: +81-6-6850-5779. Fax: +81-6-6850-5785. E-mail: ueda@ch.wani.osaka-u.ac.jp.). Roderick E. Wasylishen (Phone: 780-492-4336. Fax: 780-492-8231. E-mail: roderick.wasylishen@ualberta.ca.).

[†] Department of Chemistry, Graduate School of Science.

[‡] Department of Chemistry, University of Alberta.

10.1021/jp021679r CCC: $25.00

NMR investigations of materials with nanochannels and cavities at high pressures are expected to provide new insights into the local structure of a variety of porous solids.

In this study, we apply ^{129}Xe NMR to characterize the pore structure of tris(ethylenediamine) cobalt(III) chloride hydrate, (±)-$[Co(en)_3]Cl_3 \cdot nH_2O$, a traditional transition metal complex. The crystal structure has been reported for $n = 2.8$ and 3.0. The unit cell of both crystals is trigonal, $P\bar{3}c1$, and contains four formula units. The lattice parameters are $a = 1.1457 \pm 0.003$ nm and $c = 1.5482 \pm 0.006$ nm for $n = 2.8$,[43] and $a = 1.150 \pm 0.002$ nm and $c = 1.552 \pm 0.004$ nm for $n = 3.0$[44] at room temperature. This compound is racemic, consisting of Λ- and Δ-configurations of the $[Co(en)_3]^{3+}$ cation. The *c*-axis consists of stacks of $[Co(en)_3]^{3+}$ units alternating in configuration and forming a one-dimensional column. The crystal is constructed by hexagonal close packing of these columns. The interstitial space among the columns forms the nanopore, accommodating up to four water molecules per formula unit (16 molecules per unit cell). The sorption and desorption processes of the water of crystallization is "zeolitic", which is characterized macroscopically by capillary condensation. At 295 K, desorption of the waters of crystallization takes place at 0.285 kPa in the isotherm of dehydration in powder and single-crystal specimens.[45,46] Kelvin's equation led to an estimate of the pore diameter, 0.58 nm, from the characteristic pressure.[46] Single-crystal X-ray diffraction experiments suggest that the nanopore is maintained even after dehydration by heating at 120 °C, although detailed analysis of the crystal structure has not been carried out following dehydration.[44] Previously, the dynamic behavior of water in (±)-$[Co(en)_3]Cl_3 \cdot nH_2O$ has been studied by dielectric measurements[47] and solid-state NMR.[48] Furthermore, we recently reported the ability of the anhydrous complex to adsorb linear aliphatic hydrocarbons; the dynamics of the adsorbed *n*-alkanes were investigated by ^{2}H NMR.[49] Thus, the previous studies indirectly imply the existence of a nanopore that can accommodate water and/or other molecules, but detailed information about the pore structure, especially from the microscopic point of view is unavailable.

To investigate the local structure of xenon confined in (±)-$[Co(en)_3]Cl_3$ nanopores, we have carried out high-pressure ^{129}Xe NMR measurements of this intriguing material. Furthermore, we determine the chemical shift parameters of ^{129}Xe confined to the nanopore, and discuss the pore symmetry and structure on the basis of the chemical shift parameters. We also discuss the xenon−wall and xenon−xenon interactions in the (±)-$[Co(en)_3]Cl_3$ nanopore as reflected by the ^{129}Xe chemical shift parameters.

Experimental Section

Tris(ethylenediamine)cobalt(III) chloride trihydrate, (±)-$[Co(en)_3]Cl_3 \cdot 3H_2O$, was synthesized as previously described in the literature.[44] Crystals were obtained by repeating the recrystallization three times from aqueous solution. The anhydrous sample was prepared by drying (±)-$[Co(en)_3]Cl_3 \cdot nH_2O$ at 120 °C for 3 days. Before loading xenon gas, the cell containing the sample was evacuated for 2 h under reduced pressure (<1 kPa).

In-situ ^{129}Xe NMR measurements were carried out using a Bruker Model DSX-200 pulsed NMR spectrometer operating at a Larmor frequency of 55 MHz. A home-built single-channel high-pressure NMR probe was used.[15] Powdered samples were packed into a glass tube with a 5 mm outer diameter, 3.5 mm inner diameter, and 15 mm length. A small amount of glass wool was packed at the open end of the glass tube. This glass sample tube was inserted into the zirconia high-pressure cell of the probe.[15] Free induction decay (FID) signals were obtained using a single-pulse sequence. A 90° pulse width of 4 μs and a pulse delay of 10 s were used. The ^{129}Xe spin−lattice relaxation time was less than 2 s for xenon atoms confined to the pore. The number of scans varied from 512 to 8196 depending on the xenon loading. The ^{129}Xe NMR spectra were recorded at room temperature in the pressure range from 0.1 to 6.5 MPa. The ^{129}Xe chemical shifts were referenced to xenon gas at zero density ($\delta = 0.0$ ppm).[50]

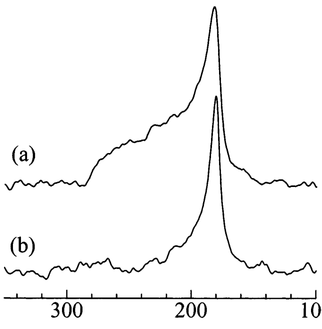

Figure 1. ^{129}Xe NMR spectra of xenon confined to the nanopores of $[Co(en)_3]Cl_3$, obtained using (a) a conventional single-pulse NMR sequence and (b) the ^{1}H to ^{129}Xe cross-polarization (CP) pulse sequence with a contact time of 7 ms. The powder specimen was sealed into a glass ampule with a xenon gas pressure of 0.33 MPa. The spectra were acquired at room temperature as described in the text.

^{1}H−^{129}Xe cross-polarization (CP) experiments were carried out using a Chemagnetics Infinity model CMX-200 pulsed NMR spectrometer with a stationary 10 mm o.d. double resonance probe. A proton 90° pulse of 4.0 μs, contact time of 7.0 ms, and repetition delays of 5 s were used for the CP experiments. The spin-locking radio frequency field was 62.5 kHz for the ^{1}H and ^{129}Xe spin system, and the maximum enhancement of the ^{129}Xe polarization was achieved by using a contact time of 7 ms. For the CP experiment, a powder sample was used which was sealed into a glass ampule with xenon gas at a pressure of 0.33 MPa.

Results and Discussion

Xe-129 NMR Spectra of (±)-$[Co(en)_3]Cl_3$. Figure 1 shows ^{129}Xe NMR spectra of xenon confined in (±)-$[Co(en)_3]Cl_3$. Xenon atoms confined to the nanochannels give rise to an axially symmetric chemical shift powder pattern characterized by $\delta_{11} = 280$ ppm and $\delta_{22} = \delta_{33} = 180$ ppm. Here, δ_{11} is the chemical shift when the external field, B_0, is along the direction of least shielding, and δ_{33} is the chemical shift when B_0 is aligned with the most shielded direction. The isotropic chemical shift δ_{iso} is given by $(1/3)(\delta_{11} + \delta_{22} + \delta_{33})$, the span Ω is represented by $\delta_{11} - \delta_{33}$, and the skew κ is $3(\delta_{22} - \delta_{iso})/(\delta_{11} - \delta_{33})$.[51] For an axially symmetric chemical shift tensor, the powder pattern is characterized by only two principal components $\delta_{\parallel}$ and $\delta_{\perp}$. In Figure 1, $\delta_{\parallel}$ and $\delta_{\perp}$ correspond to δ_{11} and $\delta_{22} = \delta_{33}$, respectively. The singularities of the powder pattern give the principal components of the shift tensor $\delta_{\perp}$ and $\delta_{\parallel}$ as 180 and 280 ppm, respectively, which correspond to a span of 100 ppm and a skew of −1.

Chemical shift anisotropy in ^{129}Xe NMR spectra has been observed for several materials with end-capped anisotropic cavities[1,24] and/or one-dimensional nanopores.[1,25−28] Observation of an isotropic peak for free xenon gas and an anisotropic ^{129}Xe NMR powder pattern for the xenon in the nanopore implies slow exchange of the xenon atoms. For a narrow and smooth channel with a diameter on the same order as the xenon van der Waals diameter, the minimum energy position for xenon is along the center of the pore cross-section.[52] In such a nanopore, the pore geometry is reflected by the symmetry of the xenon chemical shift tensor.[26,27] Thus, an axially symmetric powder pattern indicates that the compound possesses one-dimensional nanopores with cylindrical symmetry. Although these tensor components characterize the orientation of the chemical shift tensor with respect to the external magnetic field, in such a cylindrical nanopore its orientation is identical to the orientation with respect to the pore frame system. $\delta_{\parallel}$ and $\delta_{\perp}$ are then assigned to be parallel and perpendicular to the pore axis, respectively, in such systems.

To confirm the orientation of each component with respect to the crystal frame, we carried out ^{1}H$-^{129}$Xe CP experiments. For an isolated $I-S$ spin pair, the efficiency of CP depends on the magnitude of the $I-S$ heteronuclear dipolar interaction.[53] The initial rate of polarization transfer is described by the cross-relaxation rate $T_{IS}{}^{-1}$ between the $I-S$ spin pair, which is proportional to the square of the magnitude of the $I-S$ dipolar interaction. The larger the dipolar interaction, the higher the rate of polarization transfer ($T_{IS}{}^{-1}$). The heteronuclear dipolar interaction is described by the secular part of the following Hamiltonian:[54]

$$H_{IS}^{\mathrm{D}} = -R_{\mathrm{DD}}(3\cos^2\theta - 1)I_Z S_Z \tag{1}$$

where

$$R_{\mathrm{DD}} = \frac{\mu_0}{4\pi}\left(\frac{\gamma_I \gamma_S \hbar}{2\pi}\right)\langle r_{IS}^{-3}\rangle,$$

θ is the angle defining the orientation of the $I-S$ vector with respect to the external field, and $\langle r_{IS}^{-3}\rangle$ is the motionally averaged inverse cube of the internuclear distance of the $I-S$ vector. In powder samples, crystallites are distributed randomly over space, which brings about a distribution of chemical shifts. Similarly, the ^{129}Xe nuclei from each crystallite also experience different ^{1}H$-^{129}$Xe dipolar interactions, leading to a different orientation dependence on cross-relaxation rates $T_{IS}{}^{-1}$. In the case of a constant internuclear distance r_{IS}, the magnitude of the dipolar interaction depends only on the orientation of the $I-S$ vector with respect to the external field: For $\theta = 0°$, $H_{IS}^{\mathrm{D}} = -2R_{\mathrm{DD}}I_Z S_Z$, whereas for $\theta = 90°$, $H_{IS}^{\mathrm{D}} = R_{\mathrm{DD}}I_Z S_Z$. Thus for orientations corresponding to $\theta = 0°$, the absolute magnitude of the dipolar interaction is twice that for orientations with $\theta = 90°$. Because this interaction contributes to $T_{IS}{}^{-1}$ as the dipolar interaction squared, $T_{IS}{}^{-1}$ for $\theta = 0°$ is approximately four times faster than $T_{IS}{}^{-1}$ for $\theta = 90°$. Thus, the efficiency of the enhancement of the magnetization in CP depends strongly on the orientation of the dipolar interaction tensor in the principal axis system of the chemical shift tensor,[54-56] which is the same as the dependence of the dipolar interaction with respect to the external field.

In the present study, we consider the ^{1}H$-^{129}$Xe spin pair. In the nanopore of [Co(en)$_3$]Cl$_3$, the protons are present on the wall of the nanochannel. Since the protons far from a ^{129}Xe nucleus contribute little to the total dipolar interaction, the dipolar interaction contributing to the CP process will predominantly come from nearby protons. The net ^{1}H$-^{129}$Xe dipolar interaction tensor will then lie on the cross-section of the pore. That is, if the unique component of the ^{1}H$-^{129}$Xe dipolar interaction tensor is coincident with $\delta_{\parallel}$, $T_{IS}{}^{-1}$ for the peaks near $\delta_{\parallel}$ will be the fastest, leading to the largest enhancement of the magnetization at short contact times. On the other hand, if the ^{1}H$-^{129}$Xe dipolar interaction tensor is coincident with $\delta_{\perp}$, $T_{IS}{}^{-1}$ for the peaks near $\delta_{\perp}$ will be the fastest, leading to the largest enhancement of the magnetization. The ^{129}Xe NMR spectrum observed using CP showed a resonance peak without specific structure at 180 ppm as shown in Figure 1b. The chemical shift value of the peak in the CP spectrum agrees well with the perpendicular component of the chemical shift tensor $\delta_{\perp}$. Clearly the signal intensity at $\delta_{\perp}$ is enhanced more than that at $\delta_{\parallel}$ in the CP experiment. This strongly indicates that ^{129}Xe nuclei with chemical shifts near $\delta_{\perp}$ interact with protons more strongly than ^{129}Xe nuclei with chemical shifts near $\delta_{\parallel}$. According to this result, the orientation of each component of the ^{129}Xe chemical shift tensor with respect to the crystal frame can be assigned as follows: the parallel component of the chemical shift tensor $\delta_{\parallel}$ lie along the pore axis (*c*-axis), and the perpendicular components $\delta_{\perp}$ lie on the cross-section of the pore of [Co(en)$_3$]Cl$_3$, which is perpendicular to the *c*-axis. Thus, the observations from the CP experiment are consistent with the crystal symmetry and the tensor orientation on the basis of the crystal symmetry.

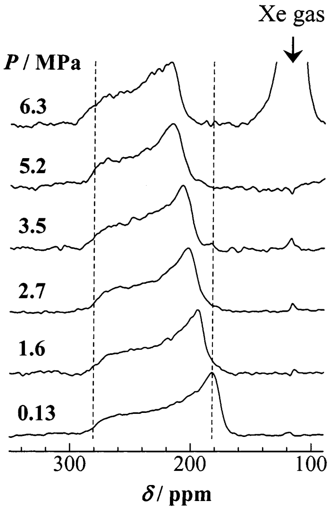

Figure 2. Pressure dependence of ^{129}Xe NMR spectra for xenon confined in the nanopores of [Co(en)$_3$]Cl$_3$. The spectrum was observed using a conventional single-pulse sequence at room temperature. For xenon gas pressures less than 6.3 mPa, the ^{129}Xe NMR peak for xenon gas had a chemical shift less than 100 ppm.

Furthermore, the ^{129}Xe NMR spectra exhibit a remarkable pressure dependence; see Figure 2. The pressure dependence of $\delta_{\perp}$, $\delta_{\parallel}$, and δ_{iso} are shown in Figure 3. As the pressure increases, $\delta_{\perp}$ increases but $\delta_{\parallel}$ appears to be almost independent of pressure.

Pressure Dependence of δ_{iso}(^{129}Xe). Extrapolating the pressure dependence of δ_{iso} to zero pressure yields δ_{iso}(0 MPa) $= 212 \pm 1$ ppm. This value reflects xenon$-$wall interactions and can be used to estimate the pore diameter. For porous silicates and aluminosilicates, Fraissard et al.[23] found an empirical correlation between the isotropic ^{129}Xe chemical shift value at zero pressure and a parameter $\bar{l}$ relating to the Xe$-$wall interaction:

$$\delta_{\mathrm{iso}}(0\ \mathrm{MPa}) = 243\frac{0.2054}{0.2054 + \bar{l}} \tag{2}$$

where $\bar{l}$ is given by $D - 0.44$ for an infinite cylinder with a diameter of D nm. Using eq 2 and δ_{iso}(0 MPa) $= 212$ ppm, the diameter of the nanopore in this compound is evaluated to be

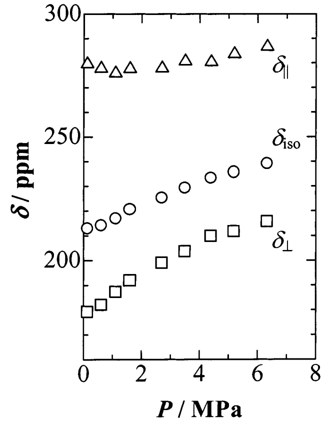

Figure 3. Pressure dependence of the isotropic chemical shift δ_{iso} and the principal components of the chemical shift tensor $\delta_{\|}$ and $\delta_{\perp}$ for xenon atoms confined in the nanopores of $[\mathrm{Co(en)_3}]\mathrm{Cl_3}$.

approximately 0.47 nm. This is much smaller than the reported diameter of 0.58 nm from the isotherm of water vapor,[46] but agrees well with the maximum diameter of 0.44 nm estimated from the crystal structure by taking into account the van der Waals radius of the hydrogen atoms (vide infra). The relationship expressed by eq 2 is based on xenon−wall interactions in the silicates and/or aluminosilicates;[23] however, for $[\mathrm{Co(en)_3}]\mathrm{Cl_3}$, the walls of the nanochannels are very different, thus xenon−wall interactions will influence the xenon magnetic shielding tensor differently. It is probably fortuitous that eq 2 yields a reasonable pore diameter for $[\mathrm{Co(en)_3}]\mathrm{Cl_3}$.

The pressure dependence of δ_{iso} is related to the xenon density in the pore, and has been interpreted in terms of the Xe−Xe interactions.[2] Figure 3 shows that the ^{129}Xe chemical shift δ_{iso} increases approximately linearly with an initial slope of 8.2×10^{-4} ppm/Torr (6.2 ppm/MPa), which is much smaller than that for other host lattices with homogeneous 1D-nanopores (vide infra).

$\mathrm{AlPO_4}$-11 is an aluminophosphate; SAPO-11 has the same framework as that of $\mathrm{AlPO_4}$-11 except that a Si atom has replaced a P or two Si atoms have replaced an Al and a P atom.[58] Both compounds have the same structure consisting of homogeneous, one-dimensional nanopores with an ellipsoidal cross section, 0.39×0.63 nm^2.[57] In both compounds, the ^{129}Xe chemical shift was observed as a function of the xenon atom loading per unit sample weight. Using the isotherms of the xenon adsorption in the nanopores of these specimens,[57] the net variation in the chemical shift as a function of the pressure is roughly estimated to be 0.13 ppm/Torr (988 ppm/MPa) for SAPO-11 and 0.04 ppm/Torr (304 ppm/MPa) for AlPO-11. The slope of the pressure dependence of δ_{iso} is related to the xenon density in the pore. Thus, the small value of the slope for $[\mathrm{Co(en)_3}]\mathrm{Cl_3}$ implies that it is difficult to load the xenon gas into these nanopores. Unfortunately, we are not equipped to measure the extent of xenon loading.

Pressure-Dependence of the Principal Components of the Chemical Shift Tensor. The values of $\delta_{\|}$ and $\delta_{\perp}$ shown in Figure 3 indicate that the ^{129}Xe nucleus is least shielded when B_0 is parallel to the nanochannels of $[\mathrm{Co(en)_3}]\mathrm{Cl_3}$. The value of $\delta_{\|}$ is relatively independent of pressure while $\delta_{\perp}$ varies from 180 ppm at the zero pressure limit to 220 ppm at the highest pressure examined here. These values lead to a span of 100 ppm at the zero pressure limit. At high pressures Ω decreases to 70 ppm. The skew $\kappa = -1$ is independent of pressure. The pressure dependence of $\delta_{\perp}$ implies that Xe−Xe interactions must be responsible for the variation of this component of the chemical shift tensor. Our observation that Xe−Xe interactions along the channel axis lead to a paramagnetic shift in $\delta_{\perp}$ (i.e., $\sigma_{\perp}$ decreases) but no change in $\delta_{\|}$ is in agreement with the recent theoretical predictions of Jameson and de Dios[59] and Jameson.[60] These authors have used ab initio magnetic shielding calculations to predict ^{129}Xe NMR line shapes for xenon confined to a variety of model nanochannels. At the zero-loading limit of a narrow bore pipe ($D_{\mathrm{pore}} \approx D_{\mathrm{Xe}}$), their results predict an axially symmetric ^{129}Xe NMR line shape with $\delta_{\|} > \delta_{\perp}$ ($\sigma_{\|} < \sigma_{\perp}$). As the xenon loading increases, the calculations indicate that the tensor component perpendicular to the axis along which the xenon atoms interact becomes less shielded, i.e., $\delta_{\perp}$ increases. The xenon shielding along the bore pipe axis is relatively insensitive to Xe−Xe interactions but rather depends on the Xe−wall interactions. At full loading, the $\sigma_{\perp}$ value is predicted to be less shielded than the $\sigma_{\|}$ value, resulting in a line shape with a skew of +1. The pressure dependence of the ^{129}Xe NMR line shape observed for $[\mathrm{Co(en)_3}]\mathrm{Cl_3}$ is that expected using the model of Jameson and de Dios; however, it is clear that even at 6 MPa, the line shape implies low Xe loading of the nanochannels.

Xe−Wall and Xe−Xe Interactions in the Pore. As mentioned above, for one-dimensional nanochannels, Xe−wall interactions should be reflected in $\delta_{\|}$. For xenon confined in $[\mathrm{Co(en)_3}]\mathrm{Cl_3}$, $\delta_{\|}$ (^{129}Xe) = 280 ppm, which is considerably larger than in analogous one-dimensional nanoporous systems such as tris(*o*-phenylenedioxy)cyclotriphosphazene (TPP).[26,27] TPP is a molecular crystal forming a hexagonal one-dimensional nanochannel with a free diameter of 0.45 nm.[26] This nanochannel has dimensions very similar to those of $[\mathrm{Co(en)_3}]\mathrm{Cl_3}$. For xenon in TPP, Pines et al. reported that $\delta_{\|} = 110$ ppm,[26,27] a value which is much smaller than that observed for $[\mathrm{Co(en)_3}]\mathrm{Cl_3}$. In other words, it appears that Xe−wall interactions in the nanochannels of $[\mathrm{Co(en)_3}]\mathrm{Cl_3}$ are greater than those in TPP (at least the xenon shielding is more perturbed in the Co(III) complex). The xenon chemical shift tensor components in $[\mathrm{Co(en)_3}]\mathrm{Cl_3}$ are closer to those of xenon in the cage of β-phenol clathrate[24] than those of xenon in TPP. β-Phenol clathrates form two types of molecular cages; one has a free diameter of 0.42 nm and is 0.67 nm long, and the other has a free diameter of 0.43 nm and is about 1.5 nm long. For the smaller cage, $\delta_{\|}$ is 343 ppm, whereas in the larger cage $\delta_{\|}$ is 320 ppm.[24] Thus, the cage diameter exactly matches the diameter of the xenon atom, bringing about large Xe−wall interactions and leading to large values of $\delta_{\|}$.

On the other hand, for one-dimensional nanochannels, Xe−Xe interactions should be reflected in $\delta_{\perp}$. Jameson and de Dios also discussed the validity of the additivity of the Xe−Xe contribution to the chemical shift.[59] In the larger cage of β-phenol clathrate, $\delta_{\perp}$ is 170 ppm for a single xenon loading, whereas $\delta_{\perp}$ is 215 ppm for the end xenon atom and 261 ppm for the central xenon atom when the cage is occupied by three xenon atoms.[24] This leads to 45 ppm as the contribution from a neighboring xenon atom close to another xenon atom to $\delta_{\perp}$.[59] On this basis, it is predicted that the $\delta_{\perp}$ value increases by about 90 ppm at full loading in a narrow pipe with a diameter corresponding to that of a xenon atom, since each xenon atom interacts with two neighbors, one on each side. However, the increase in $\delta_{\perp}$ for $[\mathrm{Co(en)_3}]\mathrm{Cl_3}$ is only 40 ppm even at 6 MPa, implying that the Xe−Xe interactions are not nearly so great as expected for xenons in close contact. In other words, the average interatomic distance between xenon atoms is longer than that predicted from the fully loaded configuration.

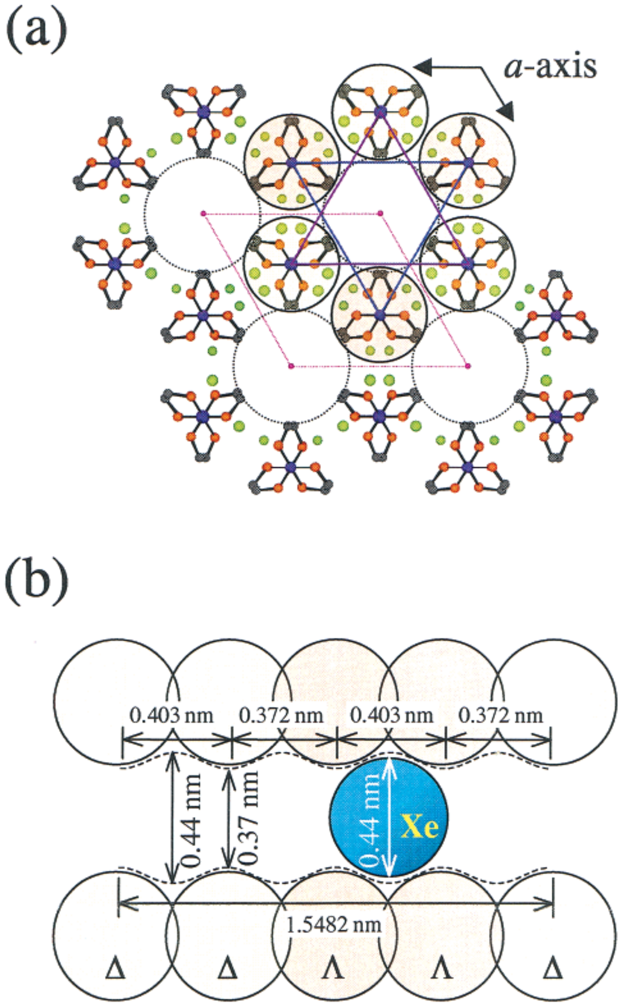

Figure 4. Schematic representation of the geometry and dimensions of the nanopore of $[Co(en)_3]Cl_3$, based on the crystal structure of $[Co(en)_3]Cl_3{\cdot}2.8H_2O$. (a) The view down the crystal *c*-axis: the $[Co(en)_3]^{3+}$ cations shaded in light orange and connected by the blue triangle lie in one plane while the three cations joined by the purple triangle lie in a different plane. (b) Slice of the nanopore along the (110) crystal plane: the maximum and minimum diameters are 0.44 and 0.37 nm, respectively. This corrugation repeats with a period of one-fourth the length of the unit cell.

The Xe−wall and Xe−Xe interactions in the $[Co(en)_3]Cl_3$/Xe system will be discussed on the basis of the pore structure of $[Co(en)_3]Cl_3$ crystal. Although the nanopore of the $[Co(en)_3]Cl_3$ crystal seems to be macroscopically homogeneous and uniform, the pore actually has a microscopic corrugation because of the atomic structure on the wall surface. Figure 4 shows a schematic representation of a pore cross-section sliced along the *c*-axis, for which the dimensions are estimated on the basis of the crystal structure of $[Co(en)_3]Cl_3{\cdot}2.8H_2O$.[43] The methylene group of ethylenediamine protrudes from the surface of the pore, and the minimum and the maximum diameters are 0.61 and 0.68 nm, respectively. Taking into account the van der Waals radius (0.12 nm) of the hydrogen atoms of the methylene group, the inner diameter of the nanopore reduces to a maximum diameter of 0.44 nm and a minimum diameter of 0.37 nm. The free diameter of this nanopore is very narrow and is comparable to the van der Waals diameter of the xenon atom, 0.432 nm. Furthermore, the corrugation of the pore depends strongly on the arrangement of the Λ- and Δ-configurations of the $[Co(en)_3]^{3+}$ cation. The $[Co(en)_3]^{3+}$ cations form a column along the *c*-axis by stacking $\Lambda(\delta\delta\delta)$ and $\Delta(\lambda\lambda\lambda)$ alternatively.[43,44] The Λ- and Δ-configurations are repeated with a *c*/2 period in a column. Considering the neighboring column, the distance between the nearest neighboring cations is different among Λ−Λ (Δ−Δ) and Λ−Δ pairs; 0.372 nm for Λ−Λ and 0.403 nm for Λ−Δ pair.[43] Since they align along the *c*-axis as follows: −Λ−Λ−Δ−Δ−Λ−Λ−Δ−Δ−, the irregularity of the pore's wall surface is repeated in the same manner. That is, there are two distances between the positions with the maximum diameter, which are 0.372 and 0.403 nm wide. Consequently, it is assumed that the xenon atoms occupy the voids with dimensions: 0.44 nm by 0.403 mm or 0.44 mm by 0.372 nm in the $[Co(en)_3]Cl_3$ crystal (see Figure 4b). This environment is very similar to the cage in β-phenol clathrate.[24] Thus, the diameter of the pore, which is of the same order as the diameter of a xenon atom, brings about the large Xe−wall interaction. Furthermore, the diameter at the bottleneck is smaller than the xenon atom. The narrow bottleneck makes the diffusion and/or migration of the xenon atom along the pore channel slow, and restricts the loading of the xenon atom into the pore. The bottleneck also repeats with periods shorter than the xenon van der Waals diameter. This makes it impossible for xenon atoms to occupy nearest-neighbor sites. Then, the Xe−Xe distances in the pore cannot be less than a half of the *c*-axis in $[Co(en)_3]Cl_3$ crystal (0.7741 nm).[43] This situation will keep the Xe−Xe interaction weak. However, the bottleneck, which is smaller than the diameter of a xenon atom, will interact effectively with xenon atoms trapped in the pore. Furthermore, the bottleneck is a circular shape with the diameter of 0.37 nm in the cross section of the pore. The interaction of a xenon atom with the bottlenecks will distort the angular momentum of the xenon atomic orbitals in the direction normal to the tangent plane, resulting in deshielding in directions both parallel and perpendicular to the pore axis. The magnitude of these paramagnetic shifts is reflected in the zero pressure shifts ($\delta_\perp = 180$ ppm, and $\delta_\parallel = 280$ ppm).

Finally, we note that the ^{129}Xe NMR powder line shape at the highest pressure (see Figure 2) is a slightly less well defined axially symmetric line shape than those obtained at lower pressures. It is possible that there is more than one unique xenon site in the nanochannels. Clearly, it would be desirable to record ^{129}Xe NMR spectra of the high-pressure samples with magic angle sample spinning.

Conclusion

To investigate the nanochannels of $[Co(en)_3]Cl_3$, we have examined the pressure dependence of ^{129}Xe NMR spectra using an in situ high-pressure NMR probe. The ^{129}Xe NMR line shape observed at each pressure is characterized by an axially symmetric chemical shift tensor, implying that this compound has a nanopore with cylindrical symmetry. The pressure dependence of δ_{iso} is weak, implying that the nanopores of $[Co(en)_3]Cl_3$ are difficult to load with xenon atoms most likely because of the very narrow channels. The cross-polarization experiment between ^{1}H and ^{129}Xe spin systems preferentially enhances the line shape at $\delta_\perp$. This observation leads to the conclusion that the orientation of $\delta_\perp$ is coincident with the ^{1}H−^{129}Xe internuclear vector. Because the orientation of the net ^{1}H−^{129}Xe internuclear vector is believed to be lying on the cross-section of the pore, the orientation of each component with respect to the pore framework can be assigned as follows: $\delta_\parallel$ is along the pore axis and $\delta_\perp$ is perpendicular to this axis. This conclusion is consistent with the orientations of chemical shift tensor determined from the symmetry of the $[Co(en)_3]Cl_3$ crystal. The maximum estimated diameter of the nanochannel, 0.44 nm, matches the diameter of the xenon atom, thus the pores interact strongly with xenon atoms, resulting in the large principal values ($\delta_{\parallel} = 280$ ppm, and $\delta_{\perp} = 180$ ppm at zero pressure limits). The pressure dependence of $\delta_{\perp}$ is attributed to Xe−Xe interactions along the channel axis. The nanochannel bottleneck with a diameter less than that of the xenon atom interacts effectively with xenon and contributes to deshielding of both principal components of the chemical shift tensor.

Acknowledgment. The authors thank members of the solid-state NMR group at the University of Alberta for several helpful comments. Also, Drs. Bob McDonald and Mike Ferguson of the X-ray Crystallography Laboratory at the University of Alberta are acknowledged. This work was partially supported by a grant-in aid for Scientific Research (No. 11440176) from the Japanese Ministry of Education, Culture, Sports, Science and Technology. We acknowledge the financial support of the Natural Sciences and Engineering Research Council (NSERC) of Canada and the University of Alberta. R.E.W. is grateful to the Government of Canada for the Canada Research Chair in Physical Chemistry at the University of Alberta.

References and Notes

(1) Ripmeester, J. A.; Ratcliffe, C. I.; Tse, J. S. *J. Chem. Soc., Faraday Trans. 1* **1988**, *84*, 3731.

(2) Ripmeester, J. A.; Ratcliffe, C. I. *J. Phys. Chem*. **1990**, *94*, 7652.

(3) Barrie, P. J.; Klinowski, J. *Prog. NMR Spectrosc.* **1992**, *24*, 91.

(4) Raftery, D.; Chmelka, B. F. *NMR: Basic Princ. Prog.* **1994**, *30*, 112.

(5) Ratcliffe, C. I. *Annu. Rep. NMR Spectrosc.* **1998**, *36*, 124.

(6) Springuel-Huet, M.-A.; Bonardet, J.-L.; Gédéon, A.; Fraissard, J. *Magn. Reson. Chem.* **1999**, *37*, S1.

(7) Moudrakovski, I. L.; Terskikh, V. V.; Ratcliffe, C. I.; Ripmeester, J. A.; Wang, L.-Q.; Shin, Y.; Exarhos, G. J. *J. Phys. Chem. B* **2002**, *106*, 5938.

(8) De Dios, A. C.; Jameson, C. J. *Annu. Rep. NMR Spectrosc.* **1994**, *29*, 1.

(9) Moudrakovski, I. L.; Sanchez, A.; Ratcliffe, C. I.; Ripmeester *J. Phys. Chem. B* **2000**, *104*, 7306.

(10) Syamala, M. S.; Cross, R. J.; Saunders, M. *J. Am. Chem. Soc.* **2002**, *124*, 6216.

(11) Kneller, J. M.; Soto, R. J.; Surber, S. E.; Colomer, J.-F.; Fonseca, A.; Nagy, J. B.; Tendeloo, G. V.; Pietrass, T. *J. Am. Chem. Soc.* **2000**, *122*, 10591.

(12) Kentgens, A. P. M.; van Boxtel, H. A.; Verweel, R.-J.; Veeman, W. S. *Macromolecules* **1991**, *24*, 3712.

(13) Tomaselli, M.; Meier, B. H.; Robyr, P.; Suter, U. W.; Ernst, R. R. *Chem. Phys. Lett.* **1993**, *205*, 145.

(14) Sperling-Ischinsky, K.; Veeman, W. S. *J. Braz. Chem. Soc.* **1999**, *10*, 299.

(15) Nagasaka, B.; Omi, H.; Eguchi, T.; Nakayama, H.; Nakamura, N. *Chem. Phys. Lett.* **2001**, *340*, 473.

(16) Ripmeester, J. A.; Ratcliffe, C. I. *J. Phys. Chem.* **1990**, *94*, 8773.

(17) Moudrakovski, I. L.; Sanchez, A. A.; Ratcliffe, C. I.; Ripmeester, J. A. *J. Phys. Chem. B* **2001**, *105*, 12338.

(18) Storhaug, V. J.; Liebig, F.; Bowers, C. R. *J. Phys. Chem. B* **2002**, *106*, 2884.

(19) Locci, E.; Dehouck, Y.; Casu, M.; Saba, G.; Lai, A.; Luhumer, M.; Reisse, J.; Bartik, K. *J. Magn. Reson.* **2001**, *150*, 167.

(20) Rubin, S. M.; Spence, M. M.; Pines, A.; Wemmer, D. E. *J. Magn. Reson.* **2001**, *152*, 79.

(21) Muenster, O.; Jokisaari, J.; Diehl, P. *Mol. Cryst. Liq. Cryst*. **1991**, *206*, 179.

(22) Bharatam, J.; Bowers, C. R. *J. Phys. Chem. B* **1999**, *103*, 2510.

(23) Demarquay, J.; Fraissard, J. *Chem. Phys. Lett*. **1987**, *136*, 314.

(24) Ripmeester, J. A. *J. Am. Chem. Soc.* **1982**, *104*, 289.

(25) Moudrakovski, I. L.; Nossov, A.; Lang, S.; Breeze, S. R.; Ratcliffe, C. I.; Simard, B.; Santyr, G.; Ripmeester, J. A. *Chem. Mater*. **2000**, *12*, 1181.

(26) Sozzani, P.; Comotti, A.; Simonutti, R.; Meersmann, T.; Logan, J. W.; Pines, A. *Angew. Chem., Int. Ed. Engl.* **2000**, *39*, 2695.

(27) Meersmann, T.; Logan, J. W.; Simonutti, R.; Caldarelli, S.; Comotti, A.; Sozzani, P.; Kaiser, L. G.; Pines, A. *J. Phys. Chem. A* **2000**, *104*, 11665.

(28) Ripmeester, J. A.; Ratcliffe, C. I. *J. Phys. Chem.* **1995**, *99*, 619.

(29) Pietraβ, T. *Magn. Reson. Rev.* **2000**, *17*, 263.

(30) Goodson, B. M. *J. Magn. Reson*. **2002**, *155*, 157.

(31) Bowers, C. R.; Long, H. W.; Pietrass, T.; Gaede, H. C.; Pines, A. *Chem. Phys. Lett.* **1993**, *205*, 168.

(32) Long, H. W.; Gaede, H. C.; Shore, J.; Reven, L.; Bowers, C. R.; Kritzenberger, J.; Pietrass, T.; Pines, A.; Tang, P.; Reimer, J. A. *J. Am. Chem. Soc.* **1993**, *115*, 8491.

(33) Albert, M. S.; Cates, G. D.; Driehuys, B.; Happer, W.; Saam, B.; Springer, C. S., Jr.; Wishnia, A. *Nature* **1994**, *370*, 199.

(34) Rõõm, T.; Appelt, S.; Seydoux, R.; Hahn, E. L.; Pines, A. *Phys. Rev. B* **1997**, *55*, 11604.

(35) Brunner, E.; Haake, M.; Pines, A.; Reimer, J. A.; Seydoux, R. *Chem. Phys. Lett*., **1998**, *290*, 112.

(36) Haake, M.; Goodson, B. M.; Laws, D. D.; Brunner, E.; Cyrier, M. C.; Havlin, R. H.; Pines, A. *Chem. Phys. Lett*. **1998**, *292*, 686.

(37) Bowers, C. R.; Storhaug, V.; Webster, C. E.; Bharatam, J.; Cottone, A., III; Gianna, R.; Betsey, K.; Gaffney, B. J. *J. Am. Chem. Soc*. **1999**, *121*, 9370.

(38) Terskikh, V. V.; Moudrakovski, I. L.; Du, H.; Ratcliffe, C. I.; Ripmeester, J. A. *J. Am. Chem. Soc*. **2001**, *123*, 10399.

(39) Appelt, S.; Haesing, F. W.; Baer-Lang, S.; Shah, N. J.; Blümich, B. *Chem. Phys. Lett.* **2001**, *348*, 263.

(40) Brunner, E.; Seydoux, R.; Haake, M.; Pines, A.; Reimer, J. A. *J. Magn. Reson.* **1998**, *130*, 145.

(41) Pietras, T.; Seydoux, R.; Pines, A. *J. Magn. Reson.* **1998**, *133*, 299.

(42) MacNamara, E.; Fisher, G.; Smith, J.; Rice, C. V.; Hwang, S.-J.; Raftery, D. *J. Phys. Chem. B* **1999**, *103*, 1158.

(43) Whuler, P. A.; Brouty, C.; Spinat, P.; Herpin, P. *Acta Crystallogr. B* **1975**, *31*, 2069.

(44) Nakatsu, K.; Saito, Y.; Kuroya, H. *Bull. Chem. Soc. Jpn.* **1956**, *29*, 428.

(45) Chihara, H.; Nakatsu, K. *Bull. Chem. Soc. Jpn.* **1959**, *32*, 903.

(46) Chihara, H. *Bull. Chem. Soc. Jpn.* **1959**, *32*, 908.

(47) Chihara, H.; Okawa, S.; Seki, S. *Bull. Chem. Soc. Jpn.* **1964**, *37*, 1373.

(48) Ueda, T.; Nakamura, N. *Z. Naturforsch. A* **2000**, *55*, 362.

(49) Nagaoka, N.; Ueda, T.; Nakamura, N. *Z. Naturforsch. A* **2002**, *57*, 435.

(50) Jameson, A. K.; Jameson, C. J.; Gutowsky, H. S. *J. Chem. Phys.* **1970**, *53*, 2310.

(51) Mason, J. *Solid State Nucl. Magn. Reson*. **1993**, *2*, 285.

(52) Cheung, T. T. P. *J. Phys. Chem.* **1995**, *99*, 7089.

(53) Mehring, M. *Principles of High-Resolution NMR in Solids*, 2nd ed.; Springer-Verlag: Berlin, 1983.

(54) Palmas, P.; Tekely, P.; Canet, D., *J. Magn. Reson*. **1993**, *104A*, 26.

(55) Muller, L.; Kumar, A.; Baumann, T.; Ernst, R. R. *Phys. Rev. Lett.* **1974**, *32*, 1402.

(56) Zilm, K. W.; Grant, D. M. *J. Am. Chem. Soc*. **1981**, *103*, 2913.

(57) Sprinuel-Huet, M. S.; Fraissard, *J. Chem. Phys. Lett*. **1989**, *154*, 299.

(58) Bennett, J. M.; Richardson Jr., J. W.; Pluth, J. J.; Smith, J. V. *Zeolites* **1987**, *7*, 160.

(59) Jameson, C. J.; de Dios, A. C. *J. Chem. Phys*. **2002**, *116*, 3805.

(60) Jameson, C. J. *J. Chem. Phys*. **2002**, *116*, 8912.